

Design of a Resistively Loaded Vee Dipole for Ultrawide-Band Ground-Penetrating Radar Applications

Kangwook Kim, *Member, IEEE*, and Waymond R. Scott, Jr., *Senior Member, IEEE*

Abstract—A new resistively loaded vee dipole (RVD) is designed and implemented for ultrawide-band short-pulse ground-penetrating radar (GPR) applications. The new RVD is improved in terms of voltage standing wave ratio, gain, and front-to-back ratio while maintaining many advantages of the typical RVD, such as the ability to radiate a short-pulse into a small spot on the ground, a low radar cross section, applicability in an array, etc. The improvements are achieved by curving the arms and modifying the Wu–King loading profile. The curve and the loading profile are designed to decrease the reflection at the drive point of the antenna while increasing the forward gain. The new RVD is manufactured by printing the curved arms on a thin Kapton film and loading them with chip resistors, which approximate the continuous loading profile. The number of resistors is chosen such that the resonant frequency due to the resistor spacing occurs at a frequency higher than the operation bandwidth. The antenna and balun are made in a module by sandwiching them between two blocks of polystyrene foam, attaching a plastic support, and encasing the foam blocks in heat-sealable plastic. The antenna module is mechanically reliable without significant performance degradation. The use of the new RVD module in a GPR system is also demonstrated with an experiment.

Index Terms—Dipole antennas, ground-penetrating radar (GPR), loaded antennas, ultrawide-band (UWB) antennas.

I. INTRODUCTION

A RESISTIVELY loaded vee dipole (RVD) is a vee antenna with both arms straight and loaded with a resistive profile [1], [2]. The RVD is usually loaded according to the Wu–King (WK) resistive profile, i.e., the conductivity is linearly tapered from the feed point to the open end of the antenna [3], [5]. Ideally, the WK profile makes the current on the antenna arms travel without internal or open-end reflections, and stabilizes the input impedance over a wide bandwidth at the expense of the radiation efficiency. The low radiation efficiency is not an important issue in applications such as the ultrawide-band (UWB), short-pulse ground-penetrating radar (GPR) systems, where the

antenna operates in close proximity to the target. In such applications, the signal to clutter ratio is more important.

The RVD with the WK profile has many advantages for use in short-pulse GPR applications [7]–[10]. The RVD can radiate a temporally-short pulse into a small spot on the ground. The radiated pulse is simply related to the input pulse, e.g., a derivative. The RVD has a low backscattering radar cross section (RCS). The low RCS minimizes multiple reflections between the ground and the antenna that can mask the signal from the target. In addition, the structure of the RVD is lightweight and suitable for an array. Thus, the RVD could be used in a hand-held system with a small number of elements or in a vehicle-mounted system with a large number of elements.

However, the typical RVD has a few drawbacks for use in a GPR system. The RVD is poorly matched to the feed line, and, thus, the voltage standing wave ratio (VSWR) is large. The reason for this is that the incident pulse in the feed line is significantly reflected at the drive point, where the pulse experiences a sudden change in the geometry, i.e., from parallel perfect electric conductors (PECs) to a resistively loaded vee. Another drawback is that it is difficult to build a mechanically-strong RVD with an accurate resistive profile in a way that does not significantly degrade its performance. We have previously developed ways to build a mechanically-strong RVD with an accurate resistive profile and demonstrated its performance [11]–[13]. In these papers, the antenna arms are printed on a thin Kapton film, and surface-mount chip resistors are loaded such that they approximate the continuous resistive profile. The antenna is then either sandwiched between two blocks of polystyrene foam or attached to a substrate. The substrate is 1.45-mm thick and cut out underneath the antenna to minimize the effect of the substrate.

In this paper, the RVD is both electrically and mechanically improved. The VSWR is improved by smoothly curving the arms from the feed line and modifying the WK profile so that the reflection at the drive point is lowered. The mechanical reliability is improved by protecting the antenna with polystyrene foam and rigidly bonding the foam and the feed line using a dielectric support structure. The new RVD is designed to operate over the target frequency range of 500 MHz to 8 GHz. The antenna is designed so that the geometry can be implemented by using printed circuit board manufacturing technology. The design process heavily relies on a numerical model, which is based on the method of moments code in the Electromagnetics Generalized (EIGER) code suite [14]. The numerical calculation was performed on a Beowulf computer cluster, which is a cluster of

Manuscript received October 19, 2004; revised March 10, 2005. This work was supported in part by the U.S. Army RDECOM CERDEC Night Vision and Electronic Sensors Directorate, Science and Technology Division, Countermine Branch and in part by the U.S. Army Research Office under Contract DAAD19-02-1-0252.

K. Kim was with the School of Electrical and Computer Engineering, Georgia Institute of Technology, Atlanta, GA 30332-0250 USA. He is now with the Samsung Advanced Institute of Technology, Yongin, Gyeonggi, South Korea (e-mail: kangwook.kim@ece.gatech.edu)

W. R. Scott is with the School of Electrical and Computer Engineering, Georgia Institute of Technology, Atlanta, GA 30332-0250 USA (e-mail: waymond.scott@ece.gatech.edu).

Digital Object Identifier 10.1109/TAP.2005.852292

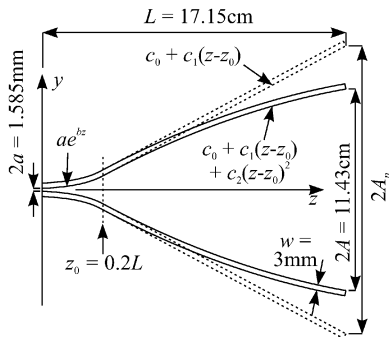


Fig. 1. Diagram of the RVD designed for GPR applications. The shape of the antenna arms, along with the loading profile, is designed to decrease the reflection at the drive point while increasing the forward gain.

standard personal computers interconnected by low cost local area network technology to provide a parallel computing environment [15]. The radiation characteristics of the new RVD and its performance as a GPR antenna are experimentally tested in the sandbox at the Electromagnetics/Acoustics Laboratory, Georgia Institute of Technology.

II. DESIGN

To make the antenna easy to fabricate, it is designed to be made on a dielectric substrate; however, the presence of the substrate can significantly degrade the performance of the antenna. To minimize the degradation caused by the substrate, the relative permittivity (ϵ_r) of the substrate must be close to $\epsilon_r = 1$, the substrate must be thin, and the conductors used for the antenna arms must be relatively wide [12]. As an example in [12], an antenna with 3-mm wide arms was implemented on a 50.8- μm thick Kapton substrate ($\epsilon_r = 3.4$). The antenna was shown to have essentially the same radiation characteristics as the antenna without a substrate but with the same geometry. Thus, in this paper, the width of the antenna arms is chosen to be $w = 3$ mm and the effect of the substrate is neglected. In addition, the antenna is fed by a 200 Ω coplanar stripline, which has conductors separated by $2a = 1.585$ mm. The coplanar stripline and the antenna can be printed on the same substrate or printed on different substrates and bonded together. The aperture length of the antenna is chosen to be $2A = 11.43$ cm, and the maximum antenna length is limited to $L_{\text{max}} = 17.15$ cm (Fig. 1).

The RVD is poorly matched to the feed line because the geometry changes abruptly and the resistance steps up at the drive point. Thus, the antenna reflects the incident pulse in the feed line significantly. To minimize the reflection, the geometry and the resistive loading are modified. The antenna arms are curved so that the geometry transitions from the feed line without discontinuity. The WK resistive profile is modified so that the onset resistance is lowered.

In Section II-A, the reflection from the exponentially curved antenna arms is investigated in the absence of the resistive loading. In Section II-B, the reflection from the resistive loading is separately investigated using a simple transmission line model. Then, the exponentially curved arms are resistively loaded, and the performance of the antenna is compared with those of the typical RVD, which has straight arms loaded with the standard WK profile. This intermediate design is

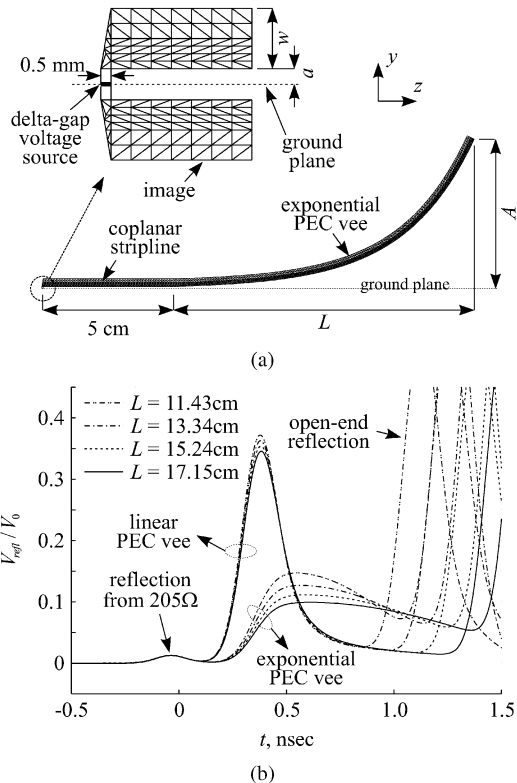


Fig. 2. (a) Mesh for the half of the geometry used in the numerical model for the exponential vee. The inclusion of the coplanar stripline allows one to separate the reflection due to the mismatch from the reflection due to the imperfection of the source model. (b) Numerical results for the reflected voltages from the exponential vees and the linear vees of different lengths.

shown to have a much lower reflection than the typical RVD. However, the amplitude of the radiated pulse is decreased. In Section II-C, a method for increasing the pulse amplitude is shown by modifying the shape of the exponentially curved arms. In Section II-D, the loading profile is discretized such that the design can be easily implemented using discrete resistors. The final design results in an antenna that has a lower drive-point reflection and radiates a stronger pulse than does the typical RVD.

A. Exponential Taper

The effects of the curved arms in the absence of the resistive loading is investigated by numerically modeling curved PEC arms and looking at the reflection at the drive point. As the smooth curve for the antenna arms, an exponential taper is first considered, which may be expressed as

$$y = ae^{bz} \quad (1)$$

where b is determined such that $y = A$ at $z = L$. Fig. 2(a) shows the mesh for the numerical model of the exponentially-curved PEC vee antenna. In this model, 5-cm long coplanar stripline is included to be able to distinguish the reflection at the antenna drive point from the reflection due to the imperfection of the source model. Note that symmetry is utilized to reduce the computational load, and, thus, only one half of the geometry is meshed. The results for the full geometry can be obtained from the results of the half geometry model by simple algebraic manipulations [2].

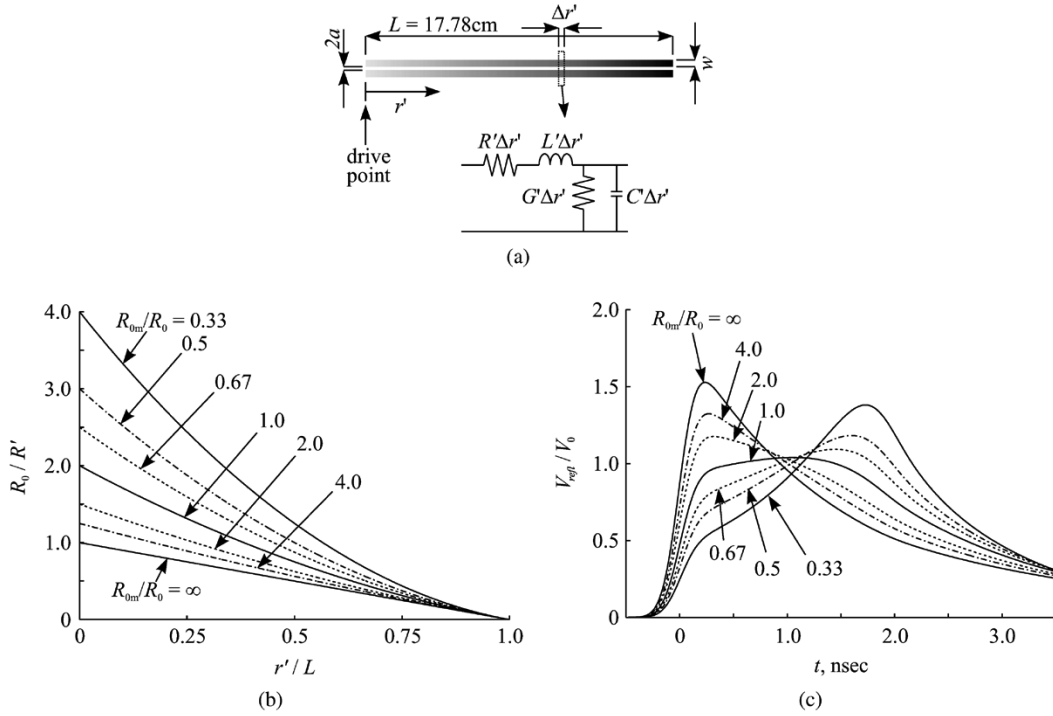


Fig. 3. Simple model for the resistively loaded coplanar stripline and its results: (a) geometry of the resistively loaded coplanar stripline and lumped-element circuit representation; (b) normalized conductance along the coplanar stripline; and (c) reflected voltages from the coplanar striplines. The curves with $R_{0m}/R_0 = \infty$ are those of the original WK profile.

The reflections are obtained for four exponential vees with lengths $L = 11.43, 13.34, 15.24,$ and 17.15 cm. For comparison, the reflections are obtained for linear PEC vees with the same lengths, which are modeled using the same modeling technique described above. The results are compared in the time domain in Fig. 2(b) when the mesh is driven by a pulse incident in a 200Ω feed line. The input pulse is a Gaussian voltage pulse, which can be expressed as

$$V_{in}(t) = V_0 \exp \left\{ -\ln 16 \left(\frac{t}{t_{FWHM}} \right)^2 \right\} \quad (2)$$

where V_0 is the amplitude, and t_{FWHM} is the full-width half-maximum of the input pulse. Here, $t_{FWHM} = 0.1765$ ns is used. In the figure, the first signal at $t = 0$ is the reflection due to the imperfection around the source. The signals near $t = 0.4$ ns are the reflections from the exponential tapers. Notice that reflections from the exponential vees are wide and low while the reflections from the linear vees are narrow and high. The reason for this is that in the exponential vee, the input pulse is continuously reflected throughout the arm while in the linear vee, the input pulse is mostly reflected at the drive point. The amplitude of the reflected pulse is lower with increasing taper length.

In Fig. 2(b), the signal at $t = 0$ is mostly the reflection from the mesh for the coplanar stripline, which is meant to be a 200Ω transmission line. In the figure, the reflection is equivalent to that from a 205Ω load. The 5Ω difference is due to the inaccuracy of the source model. The error can be lowered by increasing the mesh density at the expense of computation time. However, we believe that the accuracy of the mesh density used in the figure is enough to handle the problem of this paper because the error (2.5% relative error) is reasonably small. The meshes used in

the rest of this paper do not contain the mesh for the coplanar stripline, and they are driven directly by the source model shown in the insert in Fig. 2(a). The results have uncertainties associated with the error in the input impedance.

B. Modified Wu-King Profile

Another reason for the reflection is the discontinuity in the resistance at the drive point. The WK resistive profile in terms of the resistance per unit length is expressed as

$$R^i(r') = \frac{R_0}{1 - (r'/h)} \quad (3)$$

where r' is the distance along the arm from the drive point, h is the length of the arm, and R_0 is the resistance per unit length at the drive point. With an appropriate selection of R_0 , the current pulse injected into the RVD decreases as it travels along the arm and becomes essentially zero at the end. However, the current incident in the feed line is significantly reflected because of the resistance jump from zero in the feed line to R_0 at the drive point. Although a lower R_0 in (3) will lower the reflection at the drive point, it will lower the entire resistive profile and, therefore, result in an open-end reflection. Thus, to lower R^i at the drive point while maintaining a small open-end reflection, a modified WK profile is considered, which is expressed as

$$R_m^i(r') = \left\{ \frac{1 - (r'/h)}{R_0} + \frac{[1 - (r'/h)]^2}{R_{0m}} \right\}^{-1} \quad (4)$$

where R_{0m} is a parameter that modifies the resistive profile. Equation (4) is equivalent to (3) when $R_{0m} = \infty$. Note that $R_m^i(r' = 0)$ decreases with decreasing R_{0m} , while $R_m^i(r' = h)$ at the antenna open end always converges to $R^i(r' = h)$.

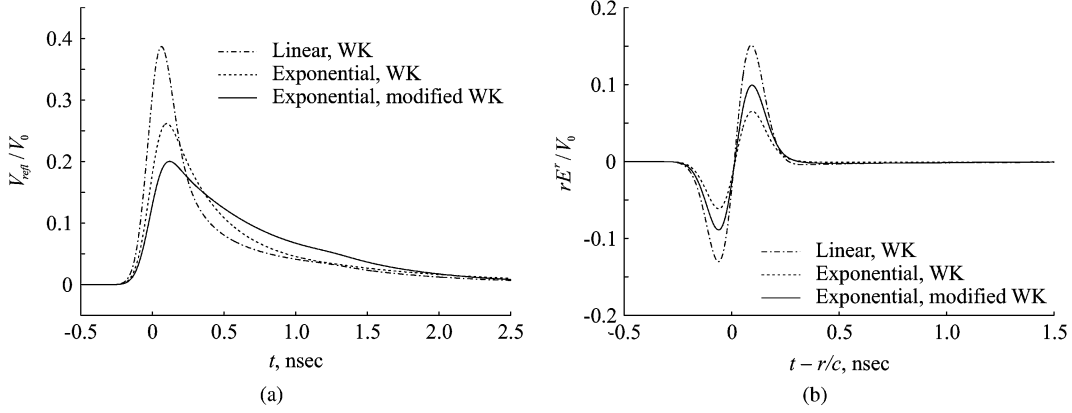


Fig. 4. Comparison of (a) the reflected voltages in the feed line and (b) the radiated fields in the forward direction for the linear vee with the original WK loading, the exponential vee with the original WK loading, and the exponential vee with the modified WK loading.

To choose an appropriate R_{0m} , a simple model was used. Fig. 3(a) shows a pair of 17.78-cm long coplanar stripline loaded with a modified WK profile. Each incremental length $\Delta r'$ of coplanar stripline can be modeled as a lumped-element circuit, which is composed of series resistance $R'\Delta r'$, series inductance $L'\Delta r'$, shunt conductance $G'\Delta r'$, and shunt capacitance $C'\Delta r'$. In this simple model, L' and C' are those of the PEC coplanar stripline, R' is that of the resistance profile, and G' is neglected, i.e.

$$\begin{aligned} L' &= \mu_0 \frac{K(m)}{K(1-m)}, & R' &= R_m^i(r') \\ C' &= \epsilon_0 \frac{K(1-m)}{K(m)}, & G' &\simeq 0 \\ m &= \frac{a}{a+w} \end{aligned} \quad (5)$$

where $K(m)$ is the complete elliptic integral of the first kind [16], [17]. The parameter $R_0h = R_0L = 467.1 \Omega$ is used throughout this paper with h being the length of the arm.

Fig. 3(b) shows seven loading profiles in terms of normalized conductance R_0/R^i , which are drawn against the distance from the drive point. The figure shows that the conductance at the drive point increases with decreasing R_{0m}/R_0 , while, at the open end of the antenna, all the conductance curves converge to the conductance curve with $R_{0m}/R_0 = \infty$, which corresponds to the original WK profile.

Fig. 3(c) shows the voltage pulses reflected from the coplanar striplines that are loaded with the profiles shown in Fig. 3(b). The input pulse is the Gaussian pulse (2) incident in a 200 Ω feed line. The figure shows that with increasing conductance at the drive point, the reflection decreases at the drive point and occurs more in the later part of the loading. The loading with $R_{0m}/R_0 = 1.0$ is seen to have the lowest amplitude in the figure.

The combined effects of the curved arms and the modified WK profile are investigated next. The exponential vee ($L = 17.15$ cm) is loaded with the modified WK profile ($R_{0m}/R_0 = 1.0$) to form the exponential vee with the modified WK loading. Fig. 4 shows the voltage reflected at the drive point and the radiated field, which are obtained numerically for the Gaussian input pulse in (2). The results are compared with those of the exponential vee with the original WK loading and the linear vee with the original WK loading (typical RVD). Fig. 4(a) shows

that the exponential vees with both the modified WK loading and the original WK loading have lower reflected voltages than the linear vee with the original WK loading in amplitude. Thus, the exponential taper lowers the amplitude when the original WK profile is used. The amplitude is further lowered by the modified WK profile, and, thus, the exponential vee with the modified WK loading has the lowest amplitude in the figure.

Fig. 4(b) shows that the exponential vee with the modified WK loading radiates a larger pulse than the exponential vee with the original WK loading. However, both exponential vees radiate a smaller pulse than the linear vee. Thus, the exponential taper performs poorly in terms of radiated pulse amplitude.

C. Curved Taper

The amplitude of the radiated pulse can be increased by modifying the exponential taper. Consider the following set of equations that describe a curve:

$$y = \begin{cases} ae^{bz}, & 0 \leq z < z_0 \\ c_0 + c_1(z - z_0) + c_2(z - z_0)^2, & z_0 \leq z \leq L. \end{cases} \quad (6)$$

Fig. 1 shows the diagram of the antenna generated by this curve. The curve grows exponentially over the interval $0 < z \leq z_0$ and grows at a slower rate over the interval $z_0 \leq z \leq L$. The parameters b , c_0 , c_1 , and c_2 are determined according to the following relations:

$$ae^{bz_0} = c_0 \quad (7a)$$

$$abe^{bz_0} = c_1 \quad (7b)$$

$$c_0 + c_1(L - z_0) = A_p \quad (7c)$$

$$c_0 + c_1(L - z_0) + c_2(L - z_0)^2 = A. \quad (7d)$$

Equations (7a) and (7b) enforce the curve is continuous and differentiable at $z = z_0$. Equation (7c) specifies half length of the aperture A_p at $z = L$ if the curve were linear over the interval $z_0 \leq z \leq L$. Equation (7d) specifies half length of the aperture A at $z = L$ with the quadratic curve.

The curve can be determined from (6) and (7) by specifying A , L , z_0 , and A_p ; A and L are determined by the maximum allowable dimensions, i.e., $2A = 11.45$ cm and $L = 17.15$ cm, and z_0 is empirically chosen to be $z_0 = 0.2L$. In Fig. 5, the reflected voltages and radiated fields are numerically obtained and plotted for four cases with $A/A_p = 0.6, 0.7, 0.8$, and 0.9 for the Gaussian input pulse defined in (2). The curves are all loaded with the modified WK profile with $R_{0m}/R_0 = 1.0$. In

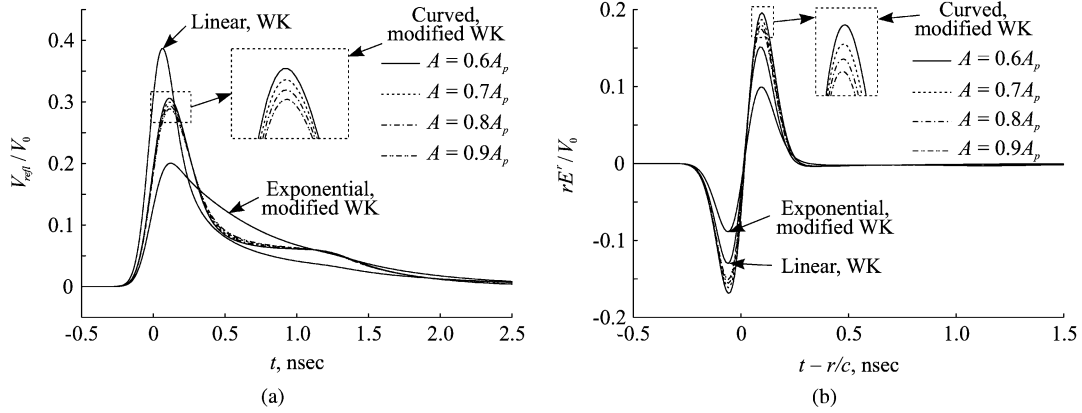


Fig. 5. Comparison of (a) the reflected voltages in the feed line and (b) the radiated fields in the forward direction for the linear vee with the original WK loading, the exponential vee with the modified WK loading, and the curved vees with the modified WK loading with $A/A_p = 0.6, 0.7, 0.8,$ and 0.9 .

the figures, the results are compared with those for the exponential vee with the modified WK loading and the linear vee with the original WK loading. The linear vee with the original WK loading is used for comparison because it is the typical form of the RVD.

Fig. 5(a) shows that the curved vees with the modified WK loading reflect more than the exponential vee with the modified WK loading but less than the linear vee with the original WK loading. Fig. 5(b) shows that the curved vees with the modified WK loading radiate pulses larger than those radiated from the exponential vee with the modified WK loading and the linear vee with the original WK loading. Thus, by using the curved taper instead of the exponential taper, both the reflection and the radiation are increased. Note that both the reflected pulse amplitude and the radiated pulse amplitude decrease with increasing A/A_p for the curved vee with the modified WK loading. This gives a tradeoff for determining A/A_p . In this paper, $A/A_p = 0.7$, or $2A_p = 16.33$ cm is chosen to be manufactured and tested. The parameters determined from (6) and (7) are $b = 67.34$, $c_0 = 0.007976$, $c_1 = 0.5371$, and $c_2 = -1.302$.

D. Discretization

To approximate the continuous loading profile with discrete resistors, the continuous loading profile must be appropriately discretized. In this paper, each antenna arm is divided into a number of sections, and a discrete resistor is placed at the center of each section so that the resistance of each section agrees with the modified WK profile. In the numerical model, each resistor is modeled by a meshed rectangle, whose width and length are 1.25 and 1.2 mm, respectively. Each rectangle is loaded with appropriate surface impedance. Fig. 6 shows the VSWRs of the curved vees that are discretely-loaded with the modified WK profile for the cases that the continuous profile is discretized with 12, 14, and 16 resistors, which result in average resistor spacing $\Delta s = 1.513, 1.297,$ and 1.135 cm, respectively. The figure shows that the antennas with discrete loading have a significantly larger VSWR at the frequencies $f_e \simeq 9.9, 12,$ and 13 GHz. The larger VSWR occurs because of the constructive

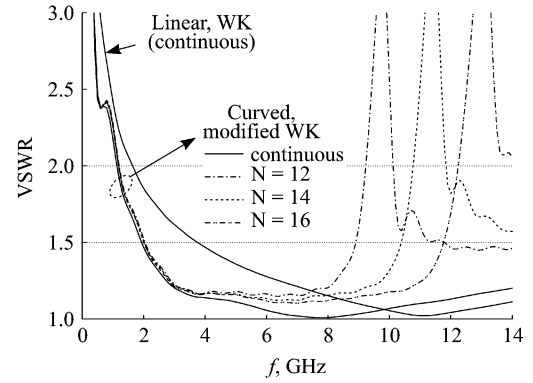


Fig. 6. VSWRs of the linear vee with the original WK loading and four curved vees with the modified WK loading. The loading profile of one curved vee is continuous, and the loading profiles of the others are discretized by $N = 12, 14,$ and 16 resistors.

interference due to the half-wavelength spacing of the resistors and can be estimated to occur at the frequency

$$f_e \simeq \frac{c}{2\Delta s}. \quad (8)$$

This frequency is inversely proportional to the resistor spacing. Thus, more resistors need to be used if one wants a broader bandwidth. However, to reduce the complexity and cost of the RVD while keeping the operating frequency band well below the resonant frequency, the discrete profile with 14 resistors is chosen.

Fig. 6 also shows the VSWR for the linear vee with the original WK loading. Notice that the VSWR is significantly lowered at low frequencies for the curved vees, essentially lowering the lower end of the bandwidth. The bandwidth with $\text{VSWR} = 2.0$ begins near 1.2 GHz for the curved vees and 1.6 GHz for the linear vee with the original WK loading. The bandwidth with $\text{VSWR} = 1.5$ begins near 2.2 GHz for the curved vees and 3.8 GHz for the linear vee with the original WK loading.

Shown in Figs. 7–9 are the comparisons of the linear vee with the original WK loading, the curved vee with continuous loading, and the curved vee with discrete loading in terms of realized gain, front-to-back ratio (F/B), and RCS. Here, the realized gain includes the losses due to the mismatch of the antenna. Fig. 7 shows that the curved vees have higher gains than the linear vee. The discretization of the loading profile does not

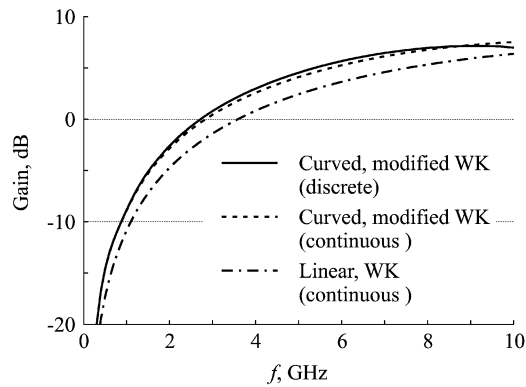


Fig. 7. Comparison of the gains of the linear vee with the original WK loading, the curved vee loaded continuously with the modified WK profile, and the curved vee loaded discretely with the modified WK profile as functions of frequency.

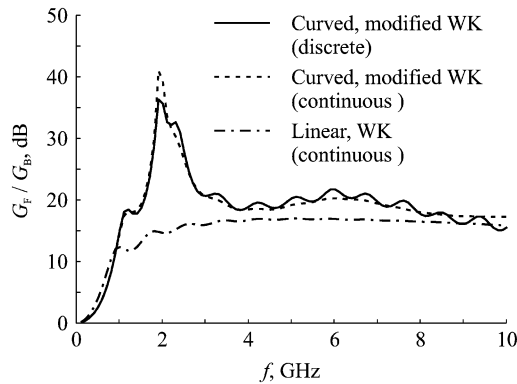


Fig. 8. Comparison of the front-to-back ratios of the linear vee with the original WK loading, the curved vee loaded continuously with the modified WK profile, and the curved vee loaded discretely with the modified WK profile.

seem to affect the gain much for frequencies less than 8 GHz. The gain of the curved vee with the discrete loading is deteriorated by the discretization at frequencies higher than 8 GHz. Note that the gains are relatively low for all the three antennas. The reason for this is that a large portion of the incident energy is dissipated in the resistors as well as reflected at the drive point [5], [18]. Thus, the radiation efficiencies of the antennas are low.

The low radiation efficiency is not an important issue in applications where the power is relatively cheap, or where the signal to clutter ratio is more important. One such application is the short-pulse GPR system, where the antenna operates in close proximity to the buried target in a cluttered environment. In short-pulse GPR, reflections from the equipment behind the antenna and multiple reflections between the antenna and the surface of the ground are bigger issues. The rejection of the signals from behind the antenna, such as the signal reflected from the equipment, can be estimated by the front-to-back ratio (F/B). Fig. 8 shows the F/Bs of the three antennas in a decibel-scale. The F/Bs of both curved vees are higher for most frequencies than that of the linear vee. The improvement is significant around 2 GHz. The improvement at 2 GHz may be particularly useful because the GPR in this work depends much on the frequency content around this frequency. The F/B of the curved vees are slightly worse than the linear vee at frequencies

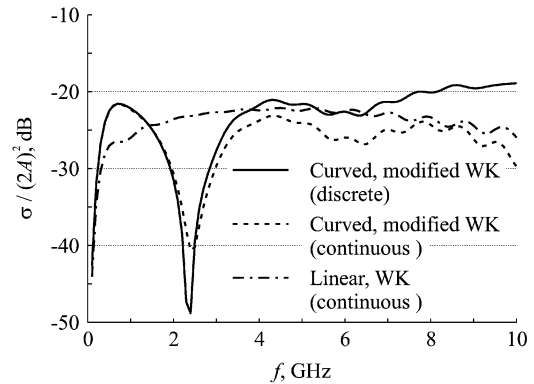


Fig. 9. Comparison of the radar cross sections for the linear vee with the original WK loading, the curved vee loaded continuously with the modified WK profile, and the curved vee loaded discretely with the modified WK profile.

lower than 0.9 GHz. The F/B for the curved vee with the discrete loading is lower than the linear vee with the original WK loading at some frequencies higher than 8 GHz due to the discretization of the loading profile.

The multiple reflections between an antenna and the surface of the ground can be lowered by designing the antenna to be less reflective, e.g., to have a low monostatic RCS for the wave incident in the front. Fig. 9 shows the monostatic RCS observed in the boresight direction of the antenna. The RCS is numerically obtained by placing a 200Ω load at the drive point and illuminating the antenna with a plane wave. The figure shows that both curved vees have larger RCSs at frequencies less than 1.5 GHz and much smaller RCSs at frequencies around 2.5 GHz than the linear vee. The RCSs of both curved vees are comparable to that of the linear vee over the frequency range $3.8 \text{ GHz} < f < 7 \text{ GHz}$.

III. IMPLEMENTATION AND EXPERIMENT

The curved vee loaded discretely with the modified WK profile has been implemented. The antenna arms are printed on a $50.8\text{-}\mu\text{m}$ thick (2 mil) flexible Kapton substrate. Each arm is loaded with 14 surface-mount chip resistors, whose width and length are 1.25 and 2.0 mm, respectively.¹ A double-Y balun, printed on a separate, 0.38-mm thick (15 mil) rigid FR-4 substrate, feeds the antenna [19], [20]. The balun transforms a 50Ω unbalanced feed line (coplanar waveguide) to a 200Ω balanced feed line (coplanar stripline).

The antenna structure made in this method is not mechanically reliable because it cannot support itself, and its components are exposed. By sandwiching the antenna and balun between two blocks of 2.54-cm thick polystyrene foam blocks, the structure can be supported and protected. However, the bonding between the antenna and the balun is still prone to damages because the thin balun can slide between the foam blocks. This problem is essentially eliminated by attaching in the back of the antenna structure a plastic support that holds both the balun and the foam. The antenna is made to a module by encasing the foam blocks in heat-sealable plastic.

¹The resistors are terminated with 0.4-mm long metal leads at both ends. Thus, the effective length of the resistive film is 1.2 mm, which is the dimension used for the length of the resistive patch in the numerical model.

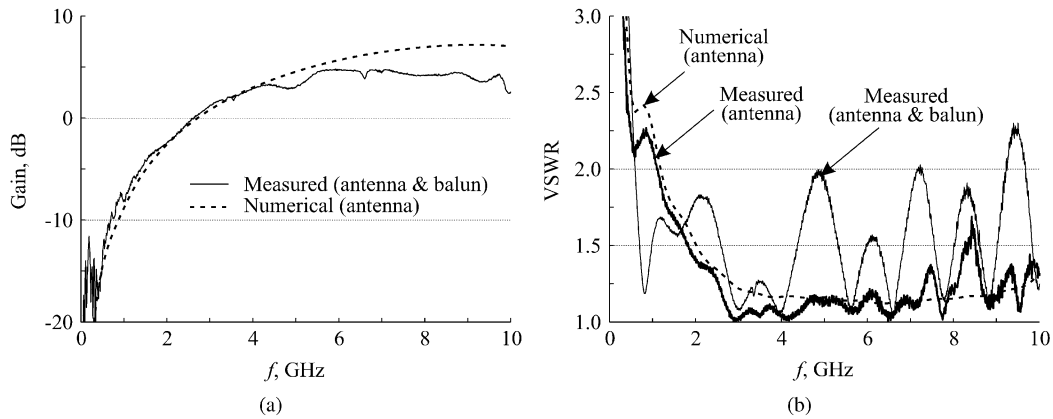


Fig. 10. Comparison of (a) measured gain and (b) VSWR with the numerical results. In the numerical model, the antenna is connected to a 200Ω feed line. In the measurement, the antenna is connected to a double-Y balun, which transforms a 50Ω coplanar waveguide to a 200Ω coplanar stripline.

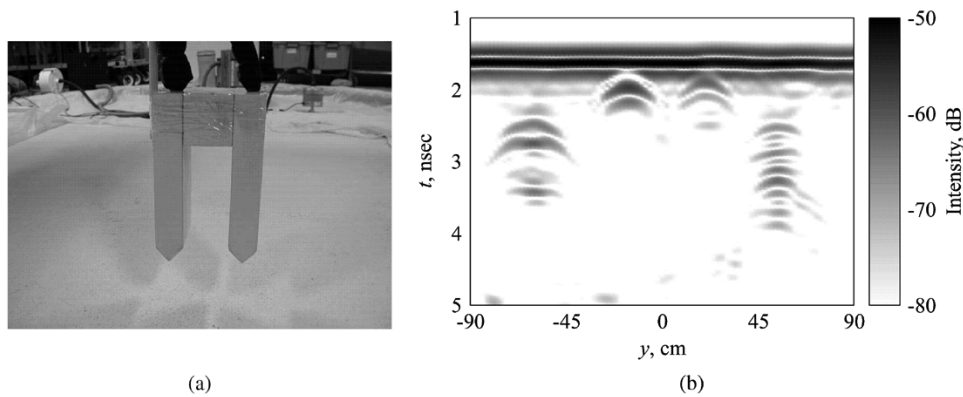


Fig. 11. (a) GPR and (b) scanned image of VS-1.6, VS-50, TS-50, and VS-2.2 at depths 6, 1, 1, and 6 cm, respectively. The result shows the signal intensities in a 30-dB scale.

The radiation characteristics of the antenna module were measured and compared with the results from the numerical model in Fig. 10. The gain graph shows that they agree well at frequencies less than 4 GHz. The performance is degraded at high frequencies due to the balun insertion loss. In Fig. 10(b), two measured VSWRs are compared with the result from the numerical model. One is measured at the balun input port in a 50Ω line so the effect of the balun is included. The other VSWR is measured in a 200Ω feed line by calibrating the balun effects out. The latter VSWR is close to that obtained numerically. The former looks much different because of the reflection from the balun and the interactions between the antenna and the balun. However, it is still under 2.0 at most frequencies.

The use of the antenna module as a GPR sensor is demonstrated in Fig. 11(a), where two identical modules are used in a bistatic configuration to increase the dynamic range. The antenna modules are separated by 11.43 cm and pointed toward the ground. Four landmines, i.e., VS-1.6, VS-50, TS-50, and VS-2.2, are used as buried targets, which are buried along the y -direction at depths 6, 1, 1, and 6 cm from the surface, respectively [21]. The targets are briefly described in Table I. The GPR is elevated approximately 2 cm off the ground. The GPR stops at 91 points with 2 cm increment as it moves along a linear path in the y -direction. At each stop, 401 equally-spaced frequency points are swept from 60 MHz to 8.06 GHz with a network analyzer. The frequency response is transformed into the time do-

TABLE I
DESCRIPTION OF TARGET LANDMINES

Name	Type	Material	Diameter	Height
VS-1.6	anti-tank	plastic	22.2 cm	9.2 cm
VS-50	anti-personnel	plastic	9 cm	4.5 cm
TS-50	anti-personnel	plastic	9 cm	4.5 cm
VS-2.2	anti-tank	plastic	24 cm	12 cm

main for an input differentiated Gaussian pulse with peak frequency $f_{pk} = 2.5$ GHz, which is expressed by

$$V_{in}(t) = \frac{V_0}{2} \omega_{pk} t \exp \left\{ \frac{1}{2} - \frac{1}{2} (\omega_{pk} t)^2 \right\} \quad (9)$$

where V_0 is the peak-to-peak amplitude, and $\omega_{pk} = 2\pi f_{pk}$.

Fig. 11(b) shows the results in a pseudo-color image, which plots the received voltage in the space-time domain. The horizontal axis represents the y -coordinate, and the vertical axis represents the time. The big horizontal response centered at 1.6 ns is the return from the surface of the ground. The landmines are clearly seen later in time. The first signals from the 1-cm deep targets are seen around 1.8 ns, and the first signals from the 6-cm deep targets are seen around 2.75 ns. The speed of wave propagation in the test soil (damp sand) is roughly a third of the speed of light in free space, or $\epsilon_r \simeq 9$. For large targets, i.e., VS-1.6 and VS-2.2, the reflections from the top and bottom of the target are distinguishable.

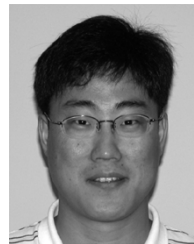
IV. CONCLUSION

A new RVD was designed and manufactured for UWB short-pulse GPR applications. The new RVD was improved from the typical RVD in terms of VSWR, gain, and F/B. The new RVD was comparable to the typical RVD in terms of RCS. The improvement was achieved by curving the arms and modifying the Wu–King resistive profile. The new RVD was implemented by printing the arms on a thin Kapton film and loading them with chip resistors. The antenna and balun were made in a module by sandwiching them between two blocks of polystyrene foam, attaching a plastic support, and encasing the foam blocks in heat-sealable plastic. The antenna module was found to be mechanically reliable without significant performance degradation. The use of the new RVD module in a GPR was also demonstrated.

The new RVD is lightweight and has a low RCS. Thus, it is suitable for an array application. The performance of a GPR system that features an array of the new RVDs could be investigated in the future. In addition, a better UWB balun needs to be designed in the future because the balun degrades the performance of the new RVD. Ideally, the new balun should have a planar geometry in order to be implemented on the same substrate as the antenna.

REFERENCES

- [1] T. P. Montoya and G. S. Smith, "Resistively loaded vee antennas for short-pulse ground-penetrating radar," in *IEEE Int. Antennas Propagat. Symp. Dig.*, Jul. 1996, pp. 2068–2071.
- [2] K. Kim, "Numerical and experimental investigation of impulse-radiating antennas for use in sensing applications," Ph.D. dissertation, Georgia Institute of Technology, Atlanta, Apr. 2003.
- [3] T. T. Wu and R. W. P. King, "The cylindrical antenna with nonreflecting resistive loading," *IEEE Trans. Antennas Propag.*, vol. AP-13, no. 3, pp. 369–373, May 1965.
- [4] L. C. Shen and R. W. P. King, "Correction to 'The cylindrical antenna with nonreflecting resistive loading'," *IEEE Trans. Antennas Propag.*, vol. 13, no. 6, p. 998, Nov. 1965.
- [5] J. G. Maloney and G. S. Smith, "A study of transient radiation from the Wu–King resistive monopole—FDTD analysis and experimental measurements," *IEEE Trans. Antennas Propag.*, vol. 41, no. 5, pp. 668–676, May 1993.
- [6] —, "Correction to 'A study of transient radiation from the Wu–King resistive monopole—FDTD analysis and experimental measurements'," *IEEE Trans. Antennas Propag.*, vol. 43, no. 2, p. 226, Feb. 1995.
- [7] T. P. Montoya and G. S. Smith, "Vee dipoles with resistive loading for short-pulse ground-penetrating radar," *Microwave Optical Tech. Lett.*, vol. 13, no. 3, pp. 132–137, Oct. 1996.
- [8] —, "Land mine detection using a ground-penetrating radar based on resistively loaded vee dipoles," *IEEE Trans. Antennas Propag.*, vol. 47, no. 12, pp. 1795–1806, Dec. 1999.
- [9] W. R. Scott Jr., K. Kim, G. D. Larson, A. C. Gurbuz, and J. H. McClellan, "Combined seismic, radar, and induction sensor for landmine detection," in *Proc. IEEE Int. Geosci. Remote Sensing Symp.*, Sep. 20–24, 2004, pp. 1613–1616.
- [10] W. R. Scott Jr., K. Kim, and G. D. Larson, "Investigation of a combined seismic, radar, and induction sensor for landmine detection," *J. Acoust. Soc. Amer.*, vol. 115, no. 5, p. 2415, May 2004.
- [11] K. Kim and W. R. Scott Jr., "Design and realization of a discretely loaded resistive vee dipole for ground-penetrating radars," *Radio Science, in the Special Section: Remote Sensing of Land Mines*, vol. 39, no. 4, Jul. 2004.
- [12] —, "Design and realization of a discretely loaded resistive vee dipole on a printed circuit board," *Detection and Remediation Technologies for Mines and Minelike Targets VIII, Proc. SPIE*, vol. 5089, pp. 818–829, Apr. 2003.
- [13] —, "A resistive linear antenna for ground-penetrating radars," *Detection and Remediation Technologies for Mines and Minelike Targets IX, Proc. SPIE*, vol. 5415, pp. 359–370, Apr. 2004.
- [14] R. M. Sharpe, J. B. Grant, N. J. Champagne, W. A. Johnson, R. E. Jorgenson, D. R. Wilton, W. J. Brown, and J. W. Rockway, "EIGER: Electromagnetic interactions generalized," in *IEEE AP-S Int. Symp. Digest*, Quebec, Canada, Jul. 1997, pp. 2366–2369.
- [15] T. L. Sterling, J. Salmon, D. J. Becker, and D. F. Savarese, *How to Build a Beowulf: A Guide to the Implementation and Application of PC Clusters*. Cambridge, MA: MIT Press, 1999.
- [16] M. Abramowitz and I. A. Stegun, *Handbook of Mathematical Functions with Formulas, Graphs, and Mathematical Tables*. Dover, New York, 1972.
- [17] W. R. Smythe, *Static and Dynamic Electricity*, 3rd ed. New York: Hemisphere, 1989, ch. 4.
- [18] M. Kanda, "A relatively short cylindrical broad-band antenna with tapered resistive loading for picosecond pulse measurements," *IEEE Trans. Antennas Propag.*, vol. 26, no. 3, pp. 439–447, May 1978.
- [19] J. B. Venkatesan and W. R. Scott Jr., "Investigation of the double-Y balun for feeding pulsed antennas," *Detection and Remediation Technologies for Mines and Minelike Targets VIII, Proc. SPIE*, vol. 5089, pp. 830–840, Apr. 2003.
- [20] —, "Design of the double-Y balun for use in GPR applications," *Detection and Remediation Technologies for Mines and Minelike Targets IX, Proc. SPIE*, vol. 5415, pp. 383–398, Apr. 2004.
- [21] Canadian Forces Landmine Database [Online]. Available: <http://ndmicidnm.forces.gc.ca>



Kangwook Kim (M'97) received the B.S. degree in electrical engineering from Ajou University, Ajou, Korea, in 1997, and the M.S. and Ph.D. degrees in electrical and computer engineering from the Georgia Institute of Technology, Atlanta, in 2001 and 2003, respectively.

From 1999 to 2003, he was a Graduate Research Assistant, and from 2003 to 2005, he was a Postdoctoral Fellow in the School of Electrical and Computer Engineering at the Georgia Institute of Technology. Since July 2005, he has been with the Samsung Advanced Institute of Technology, Yongin, Gyeonggi, South, Korea, as a Staff Researcher. His current research interests include remote sensing of concealed objects, ultrawide-band electromagnetics, and pulse antennas.



Waymond R. Scott, Jr. (S'81–M'82–SM'03) was born in Calhoun, GA, on April 6, 1958. He received the B.E.E., M.S.E.E., and Ph.D. degrees from the Georgia Institute of Technology, Atlanta, in 1980, 1982, and 1985, respectively.

From 1979 to 1980, he was a Student Assistant and Graduate Research Assistant at the Georgia Tech Research Institute, and from 1980 to 1985, he was a Graduate Research Assistant in the School of Electrical Engineering at the Georgia Institute of Technology, where he is currently a Professor of Electrical and Computer Engineering. His research interest include methods for detecting buried objects using both electromagnetic and acoustic waves, measurement of the electromagnetic properties of materials, transient electromagnetic fields, and numerical methods including the finite element and the finite-difference time-domain techniques.